Morphology of Jupiter's Polar Auroral Bright Spot Emissions via Juno-UVS Observations

K. Haewsantati[1,2,3,4], B. Bonfond[1], S. Wannawichian [3,4], G. R. Gladstone[5], V. Hue[5], M. H. Versteeg[5], T. K. Greathouse[5], D. Grodent[1], Z. Yao[6,1], W. Dunn[7,8,9], J.-C. Gérard[1], R. Giles[5], J. Kammer[5], R. Guo[1], M. F. Vogt[10]

[1]LPAP, STAR Institute, Université de Liège, Liège, Belgium
[2]Ph.D. program in Physics, Department of Physics and Materials Science, Faculty of Science, Chiang Mai University, Chiang Mai, Thailand
[3]Department of Physics and Materials Science, Faculty of Science, Chiang Mai University, Chiang Mai, Thailand
[4]National Astronomical Research Institute of Thailand (Public Organization), Chiang Mai, Thailand
[5]Southwest Research Institute, San Antonio, Texas, USA
[6]Key Laboratory of Earth and Planetary Physics, Institute of Geology and Geophysics, Chinese Academy of Sciences, Beijing, China
[7]Mullard Space Science Laboratory, Department of Space and Climate Physics, University College London, Dorking, UK
[8]The Centre for Planetary Science at UCL/Birkbeck, London, UK
[9]Harvard-Smithsonian Center for Astrophysics, Smithsonian Astrophysical Observatory, Cambridge, MA USA
[10]Center for Space Physics, Boston University, Boston, MA, USA

Key Points:

- Jupiter's auroral bright spots seen by Juno-UVS for the first 25 PJ mostly appear close to the edge of the polar-most region (swirl region).
- During long observation sequences (PJ4 and PJ16), bright spots recurred at approximately the same system III location every 22-28 minutes.
- The bright spots are not fixed at noon or at any specific local time, which possibly exclude the explanations involving a noon-facing cusp.

Corresponding author: K. Haewsantati, `K.Haewsantati@uliege.be`

Abstract

Since 2016, the Juno-UVS instrument has been taking spectral images of Jupiter's auroras during its polar fly-bys. These observations provide a great opportunity to study Jupiter's auroras in their full extent, including the nightside, which is inaccessible from Earth. We present a systematic analysis of features in Jupiter's polar auroras called auroral bright spots observed during the first 25 Juno orbits. Bright spots were identified in 16 perijoves (PJ) out of 24 (there was no available data for perijove 2), in both the northern and southern hemispheres. The emitted power of the bright spots is time variable with peak power ranging from a few tens to a hundred of gigawatts. Moreover, we found that, for some perijoves, bright spots exhibit quasiperiodic behavior. The spots, within PJ4 and PJ16, each reappeared at almost the same system III position of their first appearance with periods of 28 and 22 minutes, respectively. This period is similar to that of quasiperiodic emissions previously identified in X-rays and various other observations. The bright spot position is in a specific region in the northern hemisphere in system III, but are scattered around the magnetic pole in the southern hemisphere, near the edge of the swirl region. Furthermore, our analysis shows that the bright spots can be seen at any local time, rather than being confined to the noon sector as previously thought based on biased observations. This suggests that the bright spots might not be firmly connected to the noon facing magnetospheric cusp processes.

1 Introduction

Jupiter's very bright UV auroras result from the collision between precipitating energetic particles and the atmospheric constituents in the planet's upper atmosphere. Jupiter's UV auroras are generally divided into four components: the main emissions, the equatorward emissions, the polar emissions, and the satellites' footprints. Their specific location, morphology and behavior indicates that each of them is related to specific processes in different parts of the magnetosphere. The ever-present main emissions are the easiest feature to identify. The main emissions appear as a discontinuous contour around the magnetic pole. There is a kink region in the northern hemisphere main emission contour due to a local magnetic anomaly (Grodent et al., 2008). The main emissions are driven by internal process in the middle magnetosphere at a radial distance 20-60 Jovian radii (R_J) in the magnetosphere (Clarke et al., 2004; Vogt et al., 2011). The second component of Jupiter's aurora, the equatorward emissions, appear between the main emissions and Io's footpath and are mostly associated with magnetospheric injections (Mauk et al., 2002; Dumont et al., 2014). The multiple components of the satellite magnetic footprints are connected to the satellites of Jupiter via magnetic field lines (Bonfond, 2012). Lastly, polar auroras are characterized by the large variability of the auroral emissions in the entire region located poleward of the main emissions. The polar auroras are related to the dynamics of the outer magnetosphere, but the detailed mechanisms are still unclear. The UV polar emissions are divided into three subregions, the dark region, swirl region, and active region (Grodent et al., 2003). The dark region is characterized by its crescent shape in the dawn sector above the main emission which appears dark in ultraviolet (UV) emission (Swithenbank-Harris et al., 2019). The swirl region is a region located around the magnetic pole which consists of numerous patchy and transient features whose motion is highly variable. Despite relatively dim emissions, the swirl region usually displays spectral signatures of strong methane absorption (Bonfond, Gladstone, et al., 2017). The active region, which lies poleward from the main emission in noon to post-noon sector (Pallier & Prangé, 2001), is very dynamic. Flares, bright spots, and arc-like features are often observed in this region (Waite et al., 2001; Nichols et al., 2009; Bonfond et al., 2016).

In UV observations, one of the features of the active region studied by Pallier and Prangé (2001) is called the auroral bright spot. The bright spots that they observed in the northern hemisphere with the Hubble Space Telescope (HST) were not always observed at the same jovi-centric system III (hereafter SIII) longitude but are typically located close to noon magnetic local time. Pallier and Prangé (2001) therefore suggested that this feature is the signature of the polar cusp process. Another feature, polar flares, reported by Waite et al. (2001), were identified as short-lived but intense features in the active region that can suddenly brighten within a short time scale (10s of seconds). The flares occurring in the southern hemisphere were reported to reappear periodically with time intervals of 2-3 minutes (Bonfond et al., 2011). They were mapped to the dayside in the outer magnetosphere by using the magnetic mapping model developed by Vogt et al. (2011, 2015). Bonfond et al. (2016) revisited this study and found the quasiperiodic (QP) flares among half of their augmented dataset. These features appeared in both northern and southern hemispheres, and some of them appeared to brighten in phase. From their location, size and behaviors, the flares appear to correspond to closed field lines mapping to the dayside outer magnetosphere. Besides, the QP emissions also occur in the main emission region. Nichols, Yeoman, et al. (2017) revealed a ∼10 min period pulsating aurora feature in the main emission, which has the same period as the Alfvén wave travel time between the equatorial sheet and the ionosphere.

Quasi-periodic pulsations had been reported and studied across a wide range of datasets in the Jovian magnetosphere. For example, McKibben et al. (1993) identified 40-minute periodicity in electron bursts observed by Ulysses, with a few cases showing shorter periods (2-3 minutes). Similarly, MacDowall et al. (1993) reported two classes of QP radio bursts with periods of 15 and 40 minutes, respectively. There was also a report by Pryor et al. (2005) of the correspondence of 2 minutes long QP flares observed by Cassini Ultraviolet Imaging Spectrograph (UVIS) and low frequency radio bursts observed by Cassini Radio and Plasma Wave Spectrometer (RPWS) and Galileo Plasma Wave Spectrometer (PWS). Furthermore, many QP pulsations are reported from the analysis of X-ray observations with periods in range 10-100 minutes (Gladstone et al., 2002; Elsner et al., 2005; Dunn et al., 2016, 2017, 2020; Jackman et al., 2018; Weigt et al., 2020; Wibisono et al., 2020). Gladstone et al. (2002) presented the pulsation emissions from hot spot region in the northern hemisphere with 45 minutes period. Elsner et al. (2005) showed the relation between X-ray pulsations with ∼40 minutes period with Ulysses radio observation. Bunce et al. (2004) suggested that pulsed reconnection on the dayside magnetopause could be the source of the pulsations in both the X-ray and UV auroras.

In summary, the QP emissions in the active region typically found in HST observations of the UV auroras have shorter periods (2-3 minutes) than X-ray and radio QP emissions (10s of minutes). However, the maximum length for a continual observation obtain from HST is about 45 minutes which limits the longest periodicity it can detect to about 20 minutes. HST observations cannot explore the night side of the aurora and are biased toward configurations in which the magnetic pole is tilted towards the Earth. In contrast, observations from Juno allow for a complete view of the auroras, including the nightside, as well as longer time interval observations up to a few consecutive hours. Here, we present a systematic study of the bright spots observed with the ultraviolet spectrograph on board Juno (Juno-UVS) during the first 25 orbits, with a particular focus on bright spots location (Section 3.1) and their variability (Section 3.2).

2 Juno-UVS observations and processing methods

The Juno-UVS instrument is a UV photon-counting imaging spectrograph operating in the 68 to 210 nm wavelength range. There is a flat scan mirror at the entrance of the instrument, which allows it to look at targets up to ± 30°away from the Juno spin plane. Its "dog bone" shaped slit consists of three contiguous segments with fields-of-view (FOV) of 0.2°× 2.5°, 0.025°× 2°, and 0.2°× 2.5°. The data obtained from UVS consist of a list of photon detection events with X position of the photon count on the detector corresponding to the spectral dimension and the Y position of the spatial dimension along the slit (Gladstone et al., 2017; Greathouse et al., 2013; Hue et al., 2019).

The spacecraft spins every ∼30 seconds. Every spin, a spectrally resolved image can be reconstructed based on the motion of the field of view across the planet. The pointing mirror can target a different region of the aurora at each spin. The polar projected images used for this study assume that the aurora originates from a mean altitude of 400 km above 1 bar level (Bonfond et al., 2015). For further analysis, the photon counts are converted to brightness in kilo-Rayleighs (kR) which corresponds to the total unabsorbed H_2 Lyman emissions and Werner bands. The conversion can be done by multiplying the intensity obtained in the 155-162 nm spectral range with a conversion factor of 8.1, using to the H_2 synthetic spectrum calculated by Gustin et al. (2013). Then, the emitted power can be computed by multiplying the brightness with the surface area and with the mean energy of a UV photon. Uncertainty on the brightness calculation mainly comes from the in-flight calibration of the instrument effective area (Hue et al., 2019). In comparison, the uncertainty related to the shot noise is negligible here because we integrate over a relatively large region of the aurora (Gérard et al., 2019).

The bright spot feature is characterized as a distinct feature with a compact shape, which is very bright (typically more than 10 times brighter) in comparison to the surrounding area in polar region. In order to identify the area of the bright spot, we first remove a mean background emission and then we consider the region whose brightness is above twice the standard deviation of surrounding area's brightness. We then fit the shape of bright spot with an ellipse and we compute the emitted power in this ellipse. In this case, the main source of uncertainty lies in the selection of the area of interest. Hence, the uncertainty is calculated by assuming an elliptical reference area 25% smaller and then 25% larger than the best fit ellipse. To assess the evolution of the total power in the region of interest, the ellipse area is fitted based only on the images for which the bright spot can be clearly identified. Then, for a given dataset (i.e. a specific spot during a given perijove), the union of the fitted ellipses is used as a reference surface to compute the total power, so that the area of interest remains the same during the whole sequence.

3 Results

From UVS data obtained during the first 25 perijoves (PJ), the bright spots appear in both northern and southern hemispheres (Figure 1). Northern hemisphere bright spots have been identified in PJ1, PJ3, PJ6, PJ8, and PJ13. However, in our dataset, the bright spots appear more often in the southern aurora, which can be seen in PJ4, PJ8, PJ9, PJ12, PJ14, PJ15, PJ16, and PJ20-PJ24. Indeed, as Juno's orbit precesses and as Juno's apojove moves from dawn to midnight, the time interval available for observations of the northern hemisphere decreased as the mission goes. It should be noted that two bright spots which appear in the same perijove at different positions are observed in PJ3, PJ12, PJ21, and PJ23. The bright spots sometimes appear as compact small spots, with smallest surface area $3.5{\times}10^5 km^2$, and sometimes it covers a larger area ($2.07{\times}10^7 km^2$). The total power emission usually lies in the range of tens of gigawatts (GW), but some spots' power can occasionally rise up to a hundred GW (e.g. PJ16 at 01:52:04, cf. Figure 6). The summary of bright spots area, power, magnetic flux corresponding to the spot's area, and the local time in Jupiter's ionosphere are shown in Figure 2. In the next subsections, we will discuss the variability of the bright spots' power and position. As we will see, the bright spots usually reappear at almost the same position in SIII coordinates. Moreover, the time intervals between the occurrence of consecutive spots in a given perijove range from a few minutes to more than half an hour.

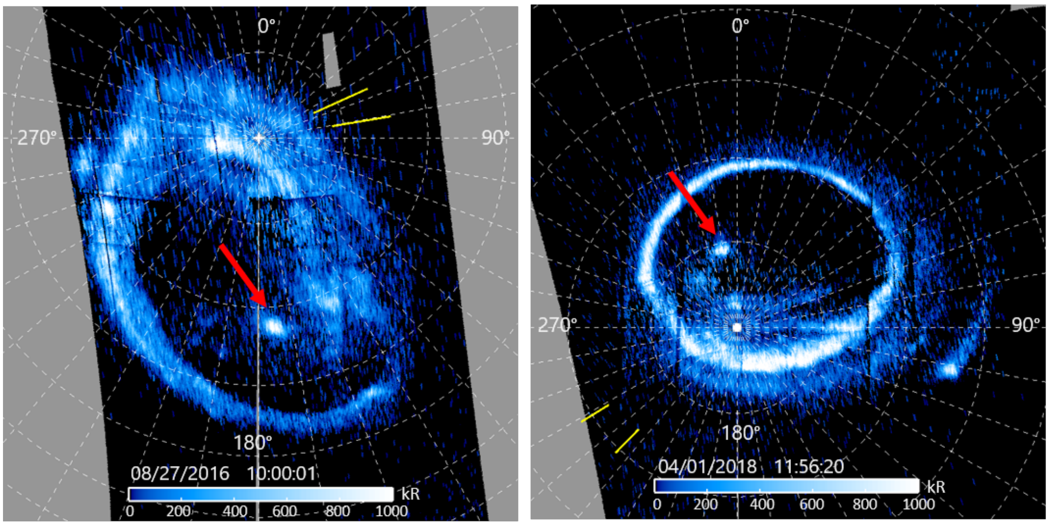

Figure 1. Two examples of bright spot in Jupiter's polar auroras (indicated by red arrows) as observed by Juno-UVS in the northern hemisphere during PJ1 (left) and the southern hemisphere during PJ12 (right). The grid represents meridians and parallels in the SIII, spaced every 10°. Each polar projection is a combination of observations acquired during several spins in order to create a full view of Jupiter's aurora. Two short-yellow lines show the subsolar longitudes of the start time and stop time of combined data.

3.1 Location and Local Time

3.1.1 Position in System III

The pixel positions of the peak of bright spots were used to calculate the latitudinal and longitudinal coordinates of spot features in the ionosphere. The bright spots in the northern hemisphere are mostly clustered in a restricted region. As shown in Figure 3, the positions of bright spots, except for PJ8 data (marked as green cross), are in range of 60-70 degrees latitude and 160-190 SIII degrees longitude. Incidentally, this region is also the X-ray hot spot regions (Gladstone et al., 2002; Dunn et al., 2016, 2017; Weigt et al., 2020; Dunn et al., 2020). One notable exception is found during PJ8, during which the bright spot is at ~ 82 degrees latitude and 216.5 degrees SIII longitude. On the other hand, the bright spots detected in the southern hemisphere scatter around the magnetic pole.

Figure 3 shows the positions of the bright spots in SIII, superimposed on the surface magnetic field strength from the JRM09 model (Connerney et al., 2018). Considering the two hemispheres together, it appears that the bright spots favour areas where the surface magnetic field is larger than 8×10^5 nT. The only exception being the bright spots observed in the north during PJ8, which is one of the dimmest of our selection. Moreover, we calculated for the solar zenith angle at the bright spots positions (see supporting information). The bright spots occur even when the sun is at high zenith angle or even below the horizon. Therefore, the bright spots might be independence on the conductivity of the ionosphere.

3.1.2 Position with respect to the swirl region

We also plot the bright spot positions over maps of the color ratio, in order to locate them with respect to the swirl region. These are produced from the ratio between

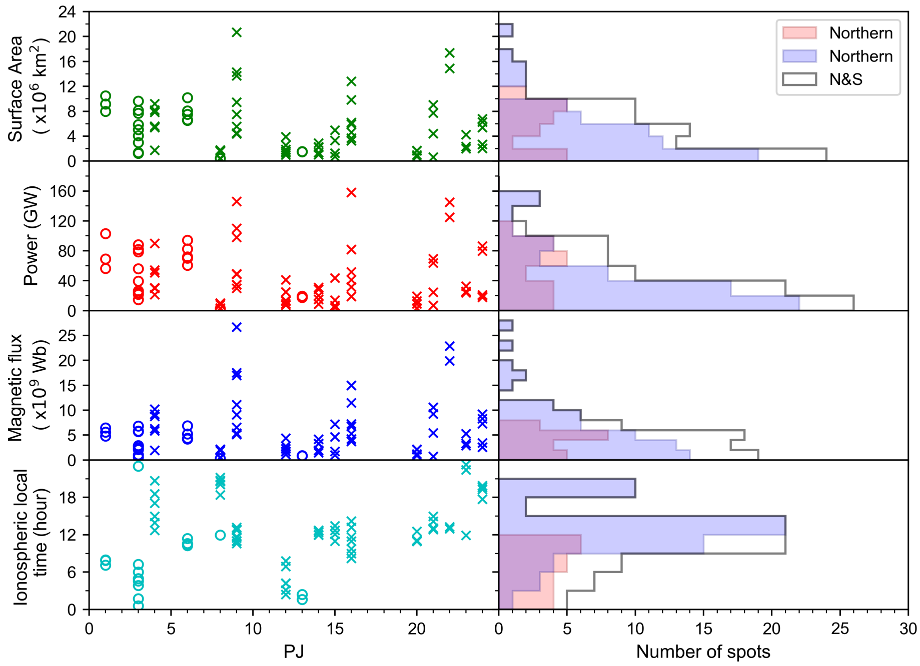

Figure 2. Top three panels are distribution of the surface area, the power emission, and the magnetic flux inside bright spot's area based on elliptical fit. Bottom panel shows ionospheric local time of bright spot's peak emission. On the left panels, those values vary at different PJs, for the northern spots (circles) and the southern spots (crosses). The total numbers of spots for each parameter from each hemisphere are presented by histogram on the right panels.

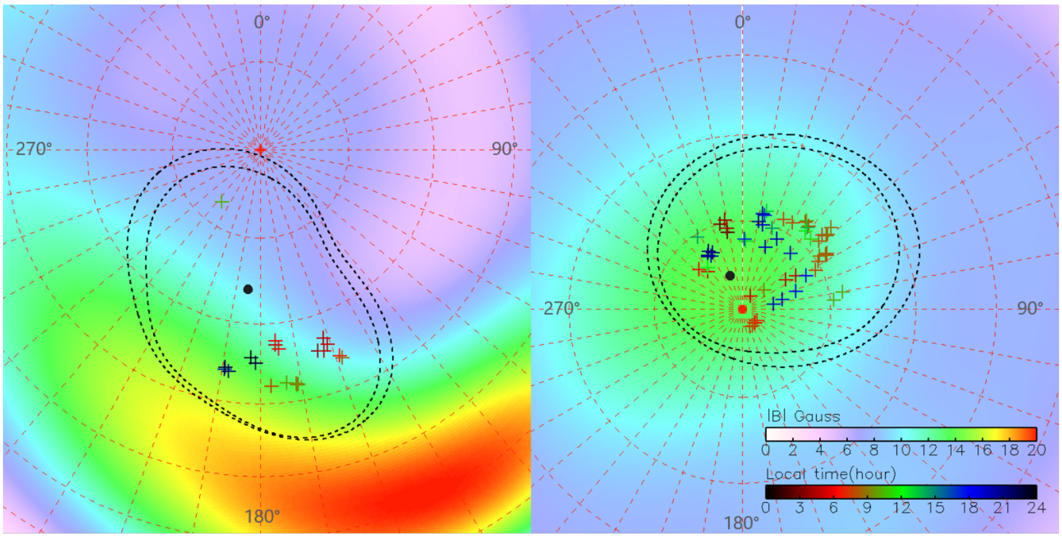

Figure 3. Polar projections with the same coordinates as Figure 1, show the magnetic field magnitude (in Gauss) on the surface of Jupiter based on JRM09 model (Connerney et al., 2018) and positions of bright spots observed in Jupiter's polar region for (left) northern and (right) southern hemispheres. The two dash contours are the statistical locations of the main emission for the compressed (inner contour) and expanded (outer contour) cases observed by HST in 2007 (Bonfond et al., 2012). The black dot indicates the magnetic pole of each hemisphere (Bonfond, Saur, et al., 2017; Connerney et al., 2018). The colors of bright spot positions correspond to their local times, acquired by magnetic mapping model developed by Vogt et al. (2011, 2015) couple with JRM09 model.

emission intensity of molecular hydrogen at two wavelength ranges, one unaffected by methane absorption (1550-1620 Å) and one affected by methane absorption (1250-1300 Å). On these maps, the swirl region displays distinctive strong absorption signatures (Bonfond, Gladstone, et al., 2017). Figure 4 shows examples of such color ratio maps from PJ6 (north, left) and PJ16 (south, right) with the position of the bright spots identified during these perijoves over-plotted. The results show that the most bright spots are located near the boundary of the high color ratio regions (swirl region). The most diverse position took place during PJ1, for which the bright spots are located inside the high color ratio region instead of at its boundary (see supporting information).

3.1.3 Position in magnetic local time

Observations carried out with HST suggested that the bright spot are located in the magnetic noon sector (Pallier & Prangé, 2001). However, HST observations are biased in favor of a configuration when the magnetic pole faces the Earth and the night side of the aurora is out of sight. On the contrary, Juno-UVS allows us to get an unbiased understanding of the mapping of the bright spots in the magnetosphere. We applied the magnetosphere-ionosphere mapping flux equivalence method of Vogt et al. (2011, 2015) couple with the JRM09 internal magnetic field model (Connerney et al., 2018) to evaluate the magnetospheric source location in the outer magnetosphere. It should be noted however that such a model is increasingly inaccurate as one moves from Ganymede's footprint path towards the pole. The bright spots are generally mapping to positions beyond 150 R_J or beyond the dayside magnetopause, which means the positions are beyond the model's limit. In order to estimate the result despite these limitations, we extrapolate the spots' position radially until we obtain a predicted position from the model. This can be done by tracing a line on the polar plot, from the magnetic pole toward the bright spot's position and keep moving equatorward until we obtain the latitude and longitude that can be mapped to a position inside the model boundary. In the southern hemisphere, we chose the point where the JRM09 magnetic field is vertical as the southern magnetic pole, at approximately -86 degrees latitude and 340 degrees SIII longitude. In the northern hemisphere, the magnetic field is so complex that there is no point where the field is vertical in the auroral polar region. Hence, we chose the barycenter of the aurora as defined in Bonfond, Saur, et al. (2017), at 74 degrees latitude and 185 degrees SIII longitude. The polar projection maps of bright spots and the corresponding magnetic local time are shown by the color of the crosses in Figure 3. The local times of the bright spots in the northern hemisphere range from late evening through midnight to late morning while the local times for bright spot in the southern hemisphere spread in entire range. Finally, the bottom panel of Figure 2 shows the distribution of the ionospheric local time, considering the magnetic pole defined above as the center and the Sun direction as noon. The distribution of ionospheric local times of bright spots is similar to the distribution of magnetic local times. This wide distribution of local times significantly contrasts with previous studies which suggested that the bright spot could correspond to noon local time facing magnetospheric cusp.

3.1.4 Bright spot's motion with time

As the appearance of the bright spots are detected, the cylindrical map of Figure 5 shows the track change in bright spot's latitude and SIII longitude. Please note that this figure shows both the northern and southern spots in the same plot which are separated by different colors. In most cases, the positions of the northern and southern spots only change slightly in both latitude and longitude (a few thousand kilometers). The exception spots whose locations vary noticeably are the northern spot from PJ3 and the southern spots from PJ9, PJ16 and PJ24. The motions of the bright spots at latitudes beyond ±85 degrees, i.e. PJ14 and PJ15, are actually very small because the positions lie close to the rotational pole. The bright spot found in PJ3(N), deep blue symbol in

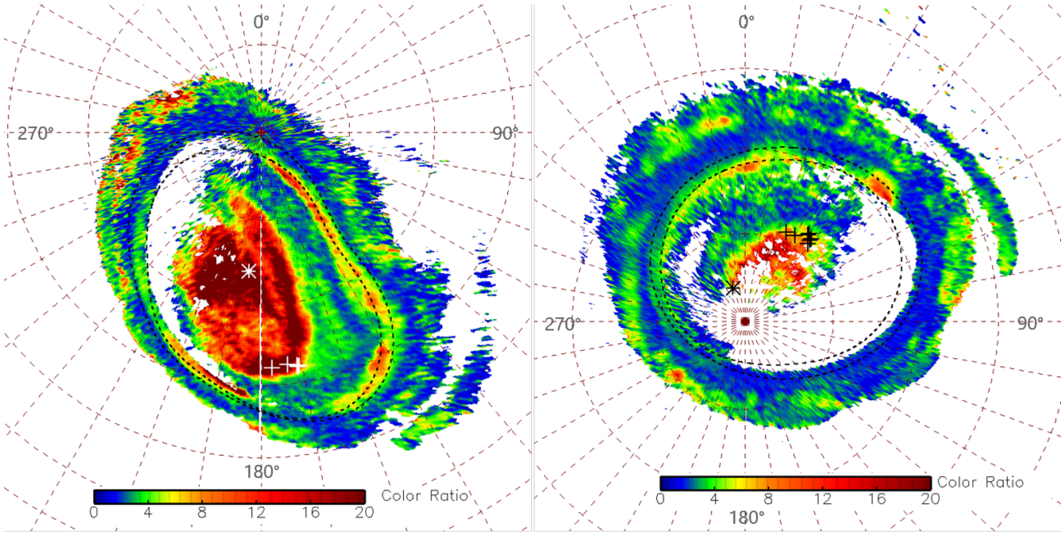

Figure 4. The bright spots positions and the color ratio map observed from (left) PJ6 and (right) PJ16. The coordinates and two dashed contours are described in Figure 1. The plus signs are the bright spots observed in (left) PJ6 and (right) PJ16. The asterisk signs represent the magnetic poles, for (left) north and (right) south hemispheres (Bonfond, Saur, et al., 2017; Connerney et al., 2018).

Figure 5, shows the variation in position starting from 164 to 158 SIII degrees longitude and 3 degrees shifted in latitude. For the bright spot in the southern hemisphere, the bright spot from PJ9 appears to move from low to high latitude starting from -76 to -80 degrees and from 47 to 62 degrees in SIII longitude while a bright spot from PJ24 continuously change position from 20 to 70 degrees longitude. These results show that the bright spots are mostly fixed in specific positions as Jupiter rotates, while, in a few cases, their positions changed. The rates of change in positions are also not related to Jupiter's rotation period. Moreover, the motions do not have any systematic pattern since we found cases where the SIII longitude increased or decreased over time.

3.2 The bright spot's power variations

Since the bright spot reappears at nearly the same position, we consider the emissions in the same region to be part of a continuous sequence. For a given perijove, the bright spots brighten and fade with a time interval on the order of minutes. When we consider the whole available dataset, this time interval is in the 3-47 minutes range.

Unfortunately, the continuous tracking of the bright spot emitted power is complicated by the fact that the field of view of the instrument varies significantly with time, which leads to discontinuous sampling rate, or inappropriately short sequences, to investigate periodicities. Moreover, as the mission progressed, the duration of the observations in the northern hemisphere decreased from a few hours to a few tens of minutes. Fortunately, two particular cases, from PJ4 and PJ16 in the South, allowed for a quasi-continuous monitoring of the bright spots' power variations for 3 to 4 hours.

Figure 6 shows the power variation as a function of time for one particular southern bright spot during PJ16 (a similar plot for PJ4 can be found in the supplemental material). The shaded areas indicate time intervals during which UVS field of view missed more than 50% of the region of interest defined by the union of the fitted ellipses. The

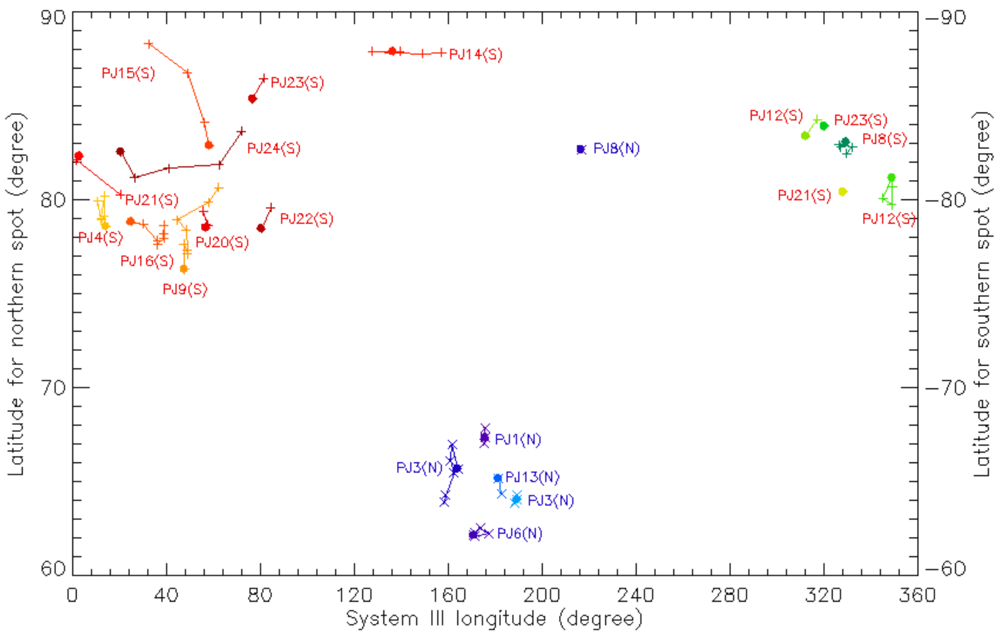

Figure 5. Latitude and SIII longitude map shows the positions of bright spot observed in northern hemisphere (plus sign) and southern hemisphere (cross sign). Each line is named by the perijove number and the hemisphere, e.g. PJ1(N) is for northern bright spot from PJ1. The northern spots are colored in shades of blue and southern spots use a color gradient from green to red. The line connecting each data presents the motion of bright spot with observing time order. The large dot for each line represents the first position of the bright spot during a sequence.

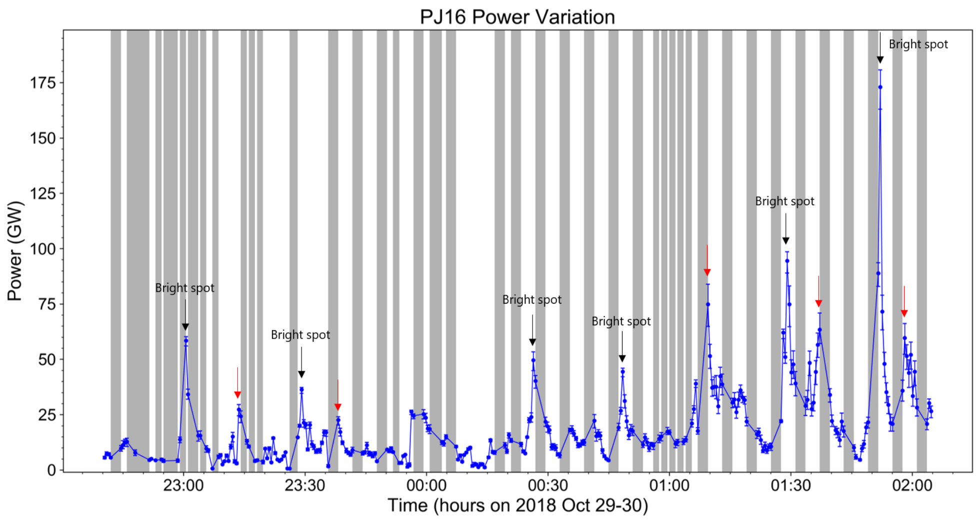

Figure 6. The time variation of power emission observed in PJ16 from 22:40:00 UT on 29 Oct 2018 to 02:00:00 UT on 30 Oct 2018. The gray boxes illustrate the times that the bright spot region was not covered by the UVS field of view. Black arrows indicate the times when clear bright spots are detected while red arrows show the additional peaks at which no bright spot appears in the region of interest.

power peaks of the bright spot are above 35 GW and can reach up to 170 GW. Moreover, a clear repetitive pattern is identified in the time series. In addition to the well-identified bright spots (black arrow), the plot shows that there are additional power peaks (indicated by red arrows) that correspond to more diffuse features that were not identified as bright spots at first. Nevertheless, these power peaks are close to shaded areas, suggesting that UVS might have missed the time interval during which a clear bright spot could have been identified. The time intervals between consecutive peaks in this plot ranges from 5 to 42 minutes, with a typical interval around 25 minutes. In order to get quantitative results, we also determine the spot's reappearance period with a Lomb-Scargle analysis (see supporting information). The results confirm that the bright spot emissions PJ16 repeatedly brighten with period of 23 min. Similarly, results from PJ4 show a $\sim$ 28-minute period. We note that these periods are similar to earlier reports about Jupiter's quasiperiodic phenomena (MacDowall et al., 1993; McKibben et al., 1993; Dunn et al., 2016; Jackman et al., 2018; Wibisono et al., 2020).

4 Discussions and Conclusions

Following the interpretation of Pallier and Prangé (2001), we expected that the bright spots would appear near noon magnetic local time and may correspond to the Jovian magnetospheric cusp. Instead, our results show that the bright spots can be seen in various ionospheric local times and are observed at positions mapping to a wide range of magnetic local times in the distant magnetosphere. Moreover, several bright spots were observed at different locations during the same observational sequence. We show that the bright spots mostly lie near the edge of the swirl region (with one exception during PJ1). Furthermore, we show that the bright spots often re-appear at the same SIII position during a given sequence, suggesting that the source region (wherever it is along the field line) corotates with Jupiter. Moreover, with additional results regarding the local time, these observations thus rule out a simple interpretation according to which the bright spot is a direct counterpart of a noon-facing magnetospheric cusp. However, Zhang et al. (2020) suggested that topology of the polar-most field lines could be very complex and helical, leading to atypical definition of a magnetospheric cusp for Jupiter and an unclear mapping of the field lines. Thus, we cannot confirm nor rule out that the bright spot could be related to some complex Jovian cusp processes.

Finally, our study of the variations of the emitted power shows that the bright spots are not sporadic random events, since they reoccur at nearly the same position after some typical time interval from a few minutes to a few tens of minutes. The bright spot emissions observed during PJ4 and PJ16 are particularly interesting because of the length of the observed sequence, and quasi-periodicities of 22-28 minutes are detected. Such timescales are hard to identify with the limited duration of HST observations (∼45 minutes). Even if we do not exclude a possible relationship between the bright spots and the flares, it should be noted that the periodicities identified here for the bright spots are one order of magnitude longer (∼30 minutes) than the one identified for the 2-3 minutes QP flares (Bonfond et al., 2011, 2016; Nichols, Badman, et al., 2017). Moreover, while most of the bright spots appear close to the boundary of the swirl region, the flares rather take place on the noon and dusk sides of the active region (Bonfond et al., 2016; Nichols, Badman, et al., 2017). Instead, the reappearances of bright spots several times during the same day suggest a link with other quasi-periodic behavior with similar time scales. It should be noted that the 3-47 minutes time intervals between consecutive emissions are also the same range as quasi-periodic pulsations identified in radio emissions (MacDowall et al., 1993), relativistic electrons (McKibben et al., 1993), Alfvén waves (Manners et al., 2018) and X-ray pulsations (Jackman et al., 2018; Wibisono et al., 2020). Further studies of the connection between these different phenomena will certainly provide important information concerning the processes giving rise to these emissions.

Acknowledgments

K. H. would like to grateful thank for financial support from Science Achievement Scholarship of Thailand (SAST) and Ph.D. program in Physics, Chiang Mai university. K. H. and S. W. are supported by National Astronomical Research Institute of Thailand (NARIT). B. B. is a Research Associate of the Fonds de la Recherche Scientifique - FNRS. B. B., D. G., Z. Y. and J.-C. G. acknowledge the support from the PRODEX Programme of European Space Agency (ESA). G. R. G., V. H., M. H. V., and T. K. G., are funded by the Southwest Research Institute. W. Dunn is supported by STFC research grant to UCL and SAO fellowship to Harvard-Smithsonian Centre for Astrophysics and by ESA. The data included herein are archived in NASA's Planetary Data System (`http://pds-atmospheres.nmsu.edu/data_and_services/atmospheres_data/JUNO/juno.html`). This research was partly supported by NARIT. Additional support was from Thailand Research Fund grants RTA6280002. We are grateful to NASA and contributing institutions which have made the Juno mission possible. This work was funded by NASA's New Frontiers Program for Juno via contract with the Southwest Research Institute.

References

Bonfond, B. (2012). When Moons Create Aurora: The Satellite Footprints on Giant Planets. In *Geophysical Monograph Series.* AGU. Retrieved 2020-07-08, from `https://orbi.uliege.be/handle/2268/136072` doi: 10.1029/2011GM001169

Bonfond, B., Gladstone, G. R., Grodent, D., Greathouse, T. K., Versteeg, M. H., Hue, V., ... Kurth, W. S. (2017, May). Morphology of the UV aurorae Jupiter during Juno's first perijove observations. *Geophysical Research Letters*, *44*(10), 4463–4471. Retrieved 2019-02-25, from `https://agupubs.onlinelibrary.wiley.com/doi/full/10.1002/2017GL073114` doi: 10.1002/2017GL073114

Bonfond, B., Grodent, D., Badman, S. V., Gérard, J.-C., & Radioti, A. (2016, December). Dynamics of the flares in the active polar region of Jupiter. *Geophysical Research Letters*, *43*(23), 11,963–11,970. Retrieved 2018-08-31, from https://agupubs.onlinelibrary.wiley.com/doi/abs/10.1002/2016GL071757 doi: 10.1002/2016GL071757

Bonfond, B., Grodent, D., Gérard, J.-C., Stallard, T., Clarke, J. T., Yoneda, M., ... Gustin, J. (2012, January). Auroral evidence of Io's control over the magnetosphere of Jupiter. *Geophysical Research Letters*, *39*(1). Retrieved 2018-08-31, from https://agupubs.onlinelibrary.wiley.com/doi/abs/10.1029/2011GL050253 doi: 10.1029/2011GL050253

Bonfond, B., Gustin, J., Gérard, J.-C., Grodent, D., Radioti, A., Palmaerts, B., ... Tao, C. (2015, October). The far-ultraviolet main auroral emission at Jupiter – Part 2: Vertical emission profile. *Ann. Geophys.*, *33*(10), 1211–1219. Retrieved 2018-08-31, from https://www.ann-geophys.net/33/1211/2015/ doi: 10.5194/angeo-33-1211-2015

Bonfond, B., Saur, J., Grodent, D., Badman, S. V., Bisikalo, D., Shematovich, V., ... Radioti, A. (2017, August). The tails of the satellite auroral footprints at Jupiter. *Journal of Geophysical Research: Space Physics*, *122*(8), 7985–7996. Retrieved 2018-08-31, from https://agupubs.onlinelibrary.wiley.com/doi/abs/10.1002/2017JA024370 doi: 10.1002/2017JA024370

Bonfond, B., Vogt, M. F., Gérard, J.-C., Grodent, D., Radioti, A., & Coumans, V. (2011, January). Quasi-periodic polar flares at Jupiter: A signature of pulsed dayside reconnections? *Geophysical Research Letters*, *38*(2). Retrieved 2018-08-31, from https://agupubs.onlinelibrary.wiley.com/doi/abs/10.1029/2010GL045981 doi: 10.1029/2010GL045981

Bunce, E. J., Cowley, S. W. H., & Yeoman, T. K. (2004, September). Jovian cusp processes: Implications for the polar aurora. *Journal of Geophysical Research: Space Physics*, *109*(A9). Retrieved 2018-08-31, from https://agupubs.onlinelibrary.wiley.com/doi/abs/10.1029/2003JA010280 doi: 10.1029/2003JA010280

Clarke, J. T., Grodent, D., Cowley, S. W. H., Bunce, E. J., Zarka, P., Connerney, J. E. P., & Satoh, T. (2004). Jupiter's aurora. In (pp. 639–670). Jupiter. The Planet, Satellites and Magnetosphere.

Connerney, J. E. P., Kotsiaros, S., Oliversen, R. J., Espley, J. R., Joergensen, J. L., Joergensen, P. S., ... Levin, S. M. (2018, March). A New Model of Jupiter's Magnetic Field From Juno's First Nine Orbits. *Geophysical Research Letters*, *45*(6), 2590–2596. Retrieved 2018-10-25, from https://agupubs.onlinelibrary.wiley.com/doi/abs/10.1002/2018GL077312 doi: 10.1002/2018GL077312

Dumont, M., Grodent, D., Radioti, A., Bonfond, B., & Gérard, J.-C. (2014, December). Jupiter's equatorward auroral features: Possible signatures of magnetospheric injections. *Journal of Geophysical Research: Space Physics*, *119*(12), 10,068–10,077. Retrieved 2018-09-03, from https://agupubs.onlinelibrary.wiley.com/doi/abs/10.1002/2014JA020527 doi: 10.1002/2014JA020527

Dunn, W. R., Branduardi-Raymont, G., Ray, L. C., Jackman, C. M., Kraft, R. P., Elsner, R. F., ... Coates, A. J. (2017, November). The independent pulsations of Jupiter's northern and southern X-ray auroras. *Nature Astronomy*, *1*(11), 758–764. Retrieved 2020-03-23, from https://www.nature.com/articles/s41550-017-0262-6 (Number: 11 Publisher: Nature Publishing Group) doi: 10.1038/s41550-017-0262-6

Dunn, W. R., Branduardi-Raymont, G., Elsner, R. F., Vogt, M. F., Lamy, L., Ford, P. G., ... Jasinski, J. M. (2016). The impact of an ICME on the Jovian X-ray aurora. *Journal of Geophysical Research: Space Physics*, *121*(3), 2274–2307. Retrieved 2020-03-23, from https://agupubs.onlinelibrary.wiley.com/doi/abs/10.1002/2015JA021888 (_eprint:

https://agupubs.onlinelibrary.wiley.com/doi/pdf/10.1002/2015JA021888) doi: 10.1002/2015JA021888

Dunn, W. R., Gray, R., Wibisono, A. D., Lamy, L., Louis, C., Badman, S. V., ... Kraft, R. (2020). Comparisons Between Jupiter's X-ray, UV and Radio Emissions and In-Situ Solar Wind Measurements During 2007. *Journal of Geophysical Research: Space Physics*, *125*(6), e2019JA027222. Retrieved 2020-07-13, from `https://agupubs.onlinelibrary.wiley.com/doi/abs/10.1029/2019JA027222` (_eprint: https://agupubs.onlinelibrary.wiley.com/doi/pdf/10.1029/2019JA027222) doi: 10.1029/2019JA027222

Elsner, R. F., Lugaz, N., Waite, J. H., Cravens, T. E., Gladstone, G. R., Ford, P., ... Majeed, T. (2005, January). Simultaneous Chandra X ray, Hubble Space Telescope ultraviolet, and Ulysses radio observations of Jupiter's aurora. *Journal of Geophysical Research: Space Physics*, *110*(A1). Retrieved 2018-08-31, from `https://agupubs.onlinelibrary.wiley.com/doi/abs/10.1029/2004JA010717` doi: 10.1029/2004JA010717

Gladstone, G. R., Jr, J. H. W., Grodent, D., Lewis, W. S., Crary, F. J., Elsner, R. F., ... Cravens, T. E. (2002, February). A pulsating auroral X-ray hot spot on Jupiter. *Nature*, *415*(6875), 1000–1003. Retrieved 2018-08-31, from `https://www.nature.com/articles/4151000a` doi: 10.1038/4151000a

Gladstone, G. R., Persyn, S. C., Eterno, J. S., Walther, B. C., Slater, D. C., Davis, M. W., ... Denis, F. (2017, November). The Ultraviolet Spectrograph on NASA's Juno Mission. *Space Science Reviews*, *213*(1), 447–473. Retrieved 2018-10-24, from `https://doi.org/10.1007/s11214-014-0040-z` doi: 10.1007/s11214-014-0040-z

Greathouse, T. K., Gladstone, G. R., Davis, M. W., Slater, D. C., Versteeg, M. H., Persson, K. B., ... Eterno, J. S. (2013, September). Performance results from in-flight commissioning of the Juno Ultraviolet Spectrograph (Juno-UVS). In *UV, X-Ray, and Gamma-Ray Space Instrumentation for Astronomy XVIII* (Vol. 8859, p. 88590T). International Society for Optics and Photonics. Retrieved 2018-09-10, from `https://www.spiedigitallibrary.org/conference-proceedings-of-spie/8859/88590T/Performance-results-from-in-flight-commissioning-of-the-Juno-Ultraviolet/10.1117/12.2024537.short` doi: 10.1117/12.2024537

Grodent, D., Bonfond, B., Gérard, J.-C., Radioti, A., Gustin, J., Clarke, J. T., ... Connerney, J. E. P. (2008, September). Auroral evidence of a localized magnetic anomaly in Jupiter's northern hemisphere. *Journal of Geophysical Research: Space Physics*, *113*(A9). Retrieved 2018-09-03, from `https://agupubs.onlinelibrary.wiley.com/doi/abs/10.1029/2008JA013185` doi: 10.1029/2008JA013185

Grodent, D., Clarke, J. T., Waite, J. H., Cowley, S. W. H., Gérard, J.-C., & Kim, J. (2003, October). Jupiter's polar auroral emissions. *Journal of Geophysical Research: Space Physics*, *108*(A10). Retrieved 2018-09-03, from `https://agupubs.onlinelibrary.wiley.com/doi/abs/10.1029/2003JA010017` doi: 10.1029/2003JA010017

Gustin, J., Gérard, J. C., Grodent, D., Gladstone, G. R., Clarke, J. T., Pryor, W. R., ... Ajello, J. M. (2013, September). Effects of methane on giant planet's UV emissions and implications for the auroral characteristics. *Journal of Molecular Spectroscopy*, *291*, 108–117. Retrieved 2019-02-26, from `http://www.sciencedirect.com/science/article/pii/S0022285213000441` doi: 10.1016/j.jms.2013.03.010

Gérard, J.-C., Bonfond, B., Mauk, B. H., Gladstone, G. R., Yao, Z. H., Greathouse, T. K., ... Levin, S. M. (2019). Contemporaneous Observations of Jovian Energetic Auroral Electrons and Ultraviolet Emissions by the Juno Spacecraft. *Journal of Geophysical Research: Space Physics*, *124*(11), 8298–8317. Retrieved 2020-01-22, from https://agupubs.onlinelibrary.wiley.com/doi/abs/10.1029/2019JA026862 doi: 10.1029/2019JA026862

Hue, V., Gladstone, G. R., Greathouse, T. K., Kammer, J. A., Davis, M. W., Bonfond, B., ... Byron, B. D. (2019, February). In-flight Characterization and Calibration of the Juno-ultraviolet Spectrograph (Juno-UVS). *The Astronomical Journal*, *157*(2), 90. Retrieved 2019-11-19, from https://doi.org/10.3847%2F1538-3881%2Faafb36 doi: 10.3847/1538-3881/aafb36

Jackman, C. M., Knigge, C., Altamirano, D., Gladstone, R., Dunn, W., Elsner, R., ... Ford, P. (2018). Assessing Quasi-Periodicities in Jovian X-Ray Emissions: Techniques and Heritage Survey. *Journal of Geophysical Research: Space Physics*, *123*(11), 9204–9221. Retrieved 2020-05-18, from https://agupubs.onlinelibrary.wiley.com/doi/abs/10.1029/2018JA025490 (_eprint: https://agupubs.onlinelibrary.wiley.com/doi/pdf/10.1029/2018JA025490) doi: 10.1029/2018JA025490

MacDowall, R. J., Kaiser, M. L., Desch, M. D., Farrell, W. M., Hess, R. A., & Stone, R. G. (1993, November). Quasiperiodic Jovian Radio bursts: observations from the Ulysses Radio and Plasma Wave Experiment. *Planetary and Space Science*, *41*(11), 1059–1072. Retrieved 2020-01-23, from http://www.sciencedirect.com/science/article/pii/003206339390109F doi: 10.1016/0032-0633(93)90109-F

Manners, H., Masters, A., & Yates, J. N. (2018). Standing Alfvén Waves in Jupiter's Magnetosphere as a Source of 10- to 60-Min Quasiperiodic Pulsations. *Geophysical Research Letters*, *45*(17), 8746–8754. Retrieved 2019-06-07, from https://agupubs.onlinelibrary.wiley.com/doi/abs/10.1029/2018GL078891 (tex.ids: mannersStandingAlfvenWaves2018a) doi: 10.1029/2018GL078891

Mauk, B. H., Clarke, J. T., Grodent, D., Waite, J. H., Paranicas, C. P., & Williams, D. J. (2002). Transient aurora on Jupiter from injections of magnetospheric electrons. *Nature*, *415*, 1003–1005.

McKibben, R. B., Simpson, J. A., & Zhang, M. (1993, November). Impulsive bursts of relativistic electrons discovered during Ulysses' traversal of Jupiter's dusk-side magnetosphere. *Planet. Space Sci.*, *41*, 1041–1058. doi: 10.1016/0032-0633(93)90108-E

Nichols, J. D., Badman, S. V., Bagenal, F., Bolton, S. J., Bonfond, B., Bunce, E. J., ... Yoshikawa, I. (2017). Response of Jupiter's auroras to conditions in the interplanetary medium as measured by the Hubble Space Telescope and Juno. *Geophysical Research Letters*, *44*(15), 7643–7652. Retrieved 2019-04-26, from https://agupubs.onlinelibrary.wiley.com/doi/abs/10.1002/2017GL073029 doi: 10.1002/2017GL073029

Nichols, J. D., Clarke, J. T., Gérard, J. C., & Grodent, D. (2009). Observations of Jovian polar auroral filaments. *Geophys. Res. Lett.*, *36*, 8101. doi: 10.1029/2009GL037578

Nichols, J. D., Yeoman, T. K., Bunce, E. J., Chowdhury, M. N., Cowley, S. W. H., & Robinson, T. R. (2017). Periodic Emission Within Jupiter's Main Auroral Oval. *Geophysical Research Letters*, *44*(18), 9192–9198. Retrieved 2019-03-25, from https://agupubs.onlinelibrary.wiley.com/doi/abs/10.1002/2017GL074824 doi: 10.1002/2017GL074824

Pallier, L., & Prangé, R. (2001, August). More about the structure of the high latitude Jovian aurorae. *Planetary and Space Science*, *49*(10), 1159–1173. Retrieved 2018-08-31, from http://www.sciencedirect.com/science/article/pii/S003206330100023X doi: 10.1016/S0032-0633(01)00023-X

Pryor, W. R., Stewart, A. I. F., Esposito, L. W., McClintock, W. E., Colwell, J. E., Jouchoux, A. J., ... Dougherty, M. K. (2005, November). Cassini UVIS observations of Jupiter's auroral variability. *Icarus*, *178*(2), 312–326. Retrieved 2020-05-13, from http://www.sciencedirect.com/science/article/pii/

S0019103505002265 doi: 10.1016/j.icarus.2005.05.021

Swithenbank-Harris, B. G., Nichols, J. D., & Bunce, E. J. (2019). Jupiter's Dark Polar Region as Observed by the Hubble Space Telescope During the Juno Approach Phase. *Journal of Geophysical Research: Space Physics*, *124*(11), 9094–9105. Retrieved 2020-04-11, from https://agupubs.onlinelibrary.wiley.com/doi/abs/10.1029/2019JA027306 (_eprint: https://agupubs.onlinelibrary.wiley.com/doi/pdf/10.1029/2019JA027306) doi: 10.1029/2019JA027306

Vogt, M. F., Bunce, E. J., Kivelson, M. G., Khurana, K. K., Walker, R. J., Radioti, A., ... Grodent, D. (2015, April). Magnetosphere-ionosphere mapping at Jupiter: Quantifying the effects of using different internal field models. *Journal of Geophysical Research: Space Physics*, *120*(4), 2584–2599. Retrieved 2018-08-30, from https://agupubs.onlinelibrary.wiley.com/doi/abs/10.1002/2014JA020729 doi: 10.1002/2014JA020729

Vogt, M. F., Kivelson, M. G., Khurana, K. K., Walker, R. J., Bonfond, B., Grodent, D., & Radioti, A. (2011, March). Improved mapping of Jupiter's auroral features to magnetospheric sources. *Journal of Geophysical Research: Space Physics*, *116*(A3). Retrieved 2019-02-25, from https://agupubs.onlinelibrary.wiley.com/doi/full/10.1029/2010JA016148 doi: 10.1029/2010JA016148

Waite, J. H., Gladstone, G. R., Lewis, W. S., Goldstein, R., McComas, D. J., Riley, P., ... Young, D. T. (2001). An auroral flare at Jupiter. *Nature*, *410*, 787–789.

Weigt, D. M., Jackman, C. M., Dunn, W. R., Gladstone, G. R., Vogt, M. F., Wibisono, A. D., ... Kraft, R. P. (2020). Chandra Observations of Jupiter's X-ray Auroral Emission During Juno Apojove 2017. *Journal of Geophysical Research: Planets*, *125*(4), e2019JE006262. Retrieved 2020-03-29, from https://agupubs.onlinelibrary.wiley.com/doi/abs/10.1029/2019JE006262 (_eprint: https://agupubs.onlinelibrary.wiley.com/doi/pdf/10.1029/2019JE006262) doi: 10.1029/2019JE006262

Wibisono, A. D., Branduardi-Raymont, G., Dunn, W. R., Coates, A. J., Weigt, D. M., Jackman, C. M., ... Fleming, D. (2020). Temporal and Spectral Studies by XMM-Newton of Jupiter's X-ray Auroras During a Compression Event. *Journal of Geophysical Research: Space Physics*, *125*(5), e2019JA027676. Retrieved 2020-07-10, from https://agupubs.onlinelibrary.wiley.com/doi/abs/10.1029/2019JA027676 (_eprint: https://agupubs.onlinelibrary.wiley.com/doi/pdf/10.1029/2019JA027676) doi: 10.1029/2019JA027676

Zhang, B., Delamere, P. A., Yao, Z., Bonfond, B., Lin, D., Sorathia, K. A., ... Lyon, J. G. (2020, June). How Jupiter's Unusual Magnetospheric Topology Structures Its Aurora. *arXiv e-prints*, *2006*, arXiv:2006.14834. Retrieved 2020-07-10, from http://adsabs.harvard.edu/abs/2020arXiv200614834Z